Acta Crystallographica Section D
Biological Crystallography
ISSN 0907-4449

Structure of the complex between teicoplanin and a bacterial cell-wall peptide: use of a carrier-protein approach

Nicoleta J. Economou,[a] Isaac J. Zentner,[a] Edwin Lazo,[b] Jean Jakoncic,[b] Vivian Stojanoff,[b] Stephen D. Weeks,[a]‡ Kimberly C. Grasty,[a] Simon Cocklin[a] and Patrick J. Loll[a]

[a]Department of Biochemistry and Molecular Biology, Drexel University College of Medicine, 245 North 15th Street, Philadelphia, PA 19102, USA, and [b]National Synchrotron Light Source, Brookhaven National Laboratory, Upton, NY 11973, USA

‡ Current address: Laboratory for Biocrystallography, Faculty of Pharmaceutical Sciences, University of Leuven, 3000 Leuven, Belgium.

Received 17 September 2012
Accepted 11 December 2012

PDB References: MBP-peptide fusion–teicoplanin, 3vfj; ubiquitin-peptide fusion–teicoplanin, 3vfk

Multidrug-resistant bacterial infections are commonly treated with glycopeptide antibiotics such as teicoplanin. This drug inhibits bacterial cell-wall biosynthesis by binding and sequestering a cell-wall precursor: a D-alanine-containing peptide. A carrier-protein strategy was used to crystallize the complex of teicoplanin and its target peptide by fusing the cell-wall peptide to either MBP or ubiquitin *via* native chemical ligation and subsequently crystallizing the protein–peptide–antibiotic complex. The 2.05 Å resolution MBP–peptide–teicoplanin structure shows that teicoplanin recognizes its ligand through a combination of five hydrogen bonds and multiple van der Waals interactions. Comparison of this teicoplanin structure with that of unliganded teicoplanin reveals a flexibility in the antibiotic peptide backbone that has significant implications for ligand recognition. Diffraction experiments revealed an X-ray-induced dechlorination of the sixth amino acid of the antibiotic; it is shown that teicoplanin is significantly more radiation-sensitive than other similar antibiotics and that ligand binding increases radiosensitivity. Insights derived from this new teicoplanin structure may contribute to the development of next-generation antibacterials designed to overcome bacterial resistance.

1. Introduction

The current wide use of antibiotics is giving rise to many antibiotic-resistant bacterial strains, presenting an ongoing challenge that must be met by the continual development of new therapeutics (Walsh, 2003). Recently, this challenge has been rendered more acute by the emergence of resistance to so-called 'last-resort drugs' such as vancomycin and teicoplanin, which are typically used to treat infections by pathogens that resist more commonly used antibiotics (for example, methicillin-resistant *Staphylococcus aureus* or MRSA).

Teicoplanin and vancomycin are natural products belonging to the class of drugs known as glycopeptide antibiotics. All drugs in this class bind and sequester a Lys-D-Ala-D-Ala-containing peptide of the bacterial cell wall, thereby inhibiting cell-wall biosynthesis (Perkins, 1969; Nieto & Perkins, 1971*b*). Glycopeptide antibiotics are heptapeptides containing both canonical and noncanonical amino acids, the side chains of which are covalently linked to form macrocycles. The peptide moieties are decorated by sugars and, occasionally, lipids. The glycopeptide antibiotics are divided into three groups based on their side-chain linkage patterns: groups I, II and III (Loll & Axelsen, 2000). Vancomycin contains non-aromatic amino acids at positions 1 and 3 and is classified as a group I antibiotic. Teicoplanin contains aromatic amino acids at the

corresponding positions, the side chains of which are cross-linked; as such, it belongs to group III (Fig. 1). Vancomycin and teicoplanin also differ in their carbohydrate groups; teicoplanin contains a mannose attached to amino acid 7, an *N*-acetylglucosamine attached to amino acid 6 and an *N*-acylglucosamine attached to amino acid 4, whereas vancomycin contains a glucose-vancosamine disaccharide attached to amino acid 4.

Although vancomycin is clinically the most commonly used glycopeptide antibiotic, teicoplanin is used in many countries and exhibits lower toxicity, a longer half-life and a more potent antimicrobial activity (Parenti, 1986; Verbist *et al.*, 1984). Teicoplanin binds its cell-wall peptide target with higher affinity than vancomycin and most other glycopeptide antibiotics (Nieto & Perkins, 1971*a*; Scrimin *et al.*, 1996; Malabarba, Trani *et al.*, 1989; Cooper *et al.*, 1997; Popieniek & Pratt, 1991; Arriaga *et al.*, 1990). Teicoplanin interacts with its ligand as a monomer, rather than a back-to-back dimer as does vancomycin (Beauregard *et al.*, 1995); nevertheless, teicoplanin is speculated to recognize its ligand in the same manner as vancomycin *via* five hydrogen bonds (Barna & Williams, 1984; Westwell *et al.*, 1995). One of these bonds is prevented from forming in the most commonly encountered form of vancomycin resistance, the VanA type, in which the sequence of the peptide target is changed to Lys-D-Ala-D-lactate (Handwerger *et al.*, 1992; Arthur *et al.*, 1992). This small change and the concomitant loss of a key hydrogen bond reduces the affinity of vancomycin for its target by ∼1000-fold (Bugg *et al.*, 1991). Since ligand recognition is similar for the various glycopeptide antibiotics, the VanA phenotype confers resistance against teicoplanin as well as vancomycin (Dutka-Malen *et al.*, 1990). Notably, a second vancomycin-resistance phenotype is known (VanB) in which sensitivity to teicoplanin is retained. This differential sensitivity has been explained in terms of membrane targeting mediated by the acyl tail of teicoplanin, which might limit the accessibility of the drug to the sensor kinase controlling resistance and/or induce blockades at different points in the cell-wall biosynthetic pathway

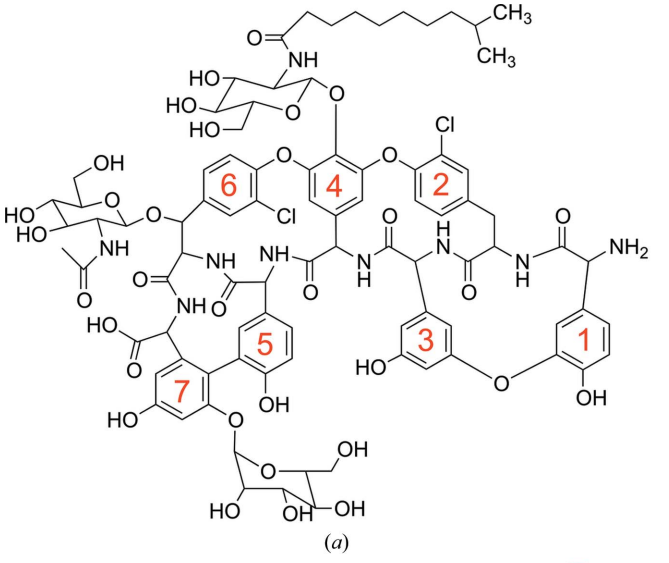

(*a*)

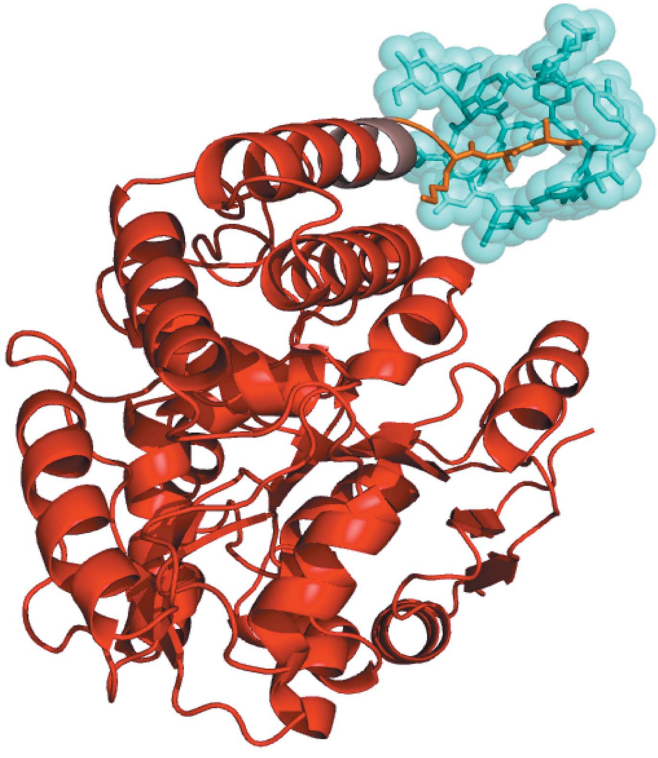

(*b*)

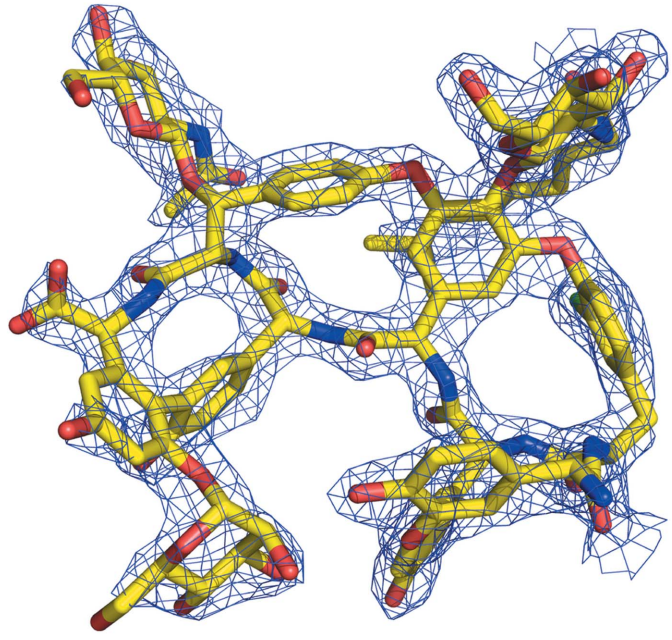

(*c*)

Figure 1
Structure of the glycopeptide antibiotic teicoplanin. (*a*) Chemical structure of teicoplanin. The seven amino acids of the peptide are numbered in red starting at the N-terminus. (*b*) Structure of teicoplanin (cyan) bound to its MBP-ligand fusion. The fusion contains an MBP carrier protein (red) covalently fused to the Lys-D-Ala-D-Ala target peptide (orange) *via* a five-alanine linker (brown). The antibiotic is shown in a stick representation, with a partially transparent surface representation overlaid. (*c*) Representative $2mF_o - DF_c$ electron density; the portion of the map shown covers the teicoplanin molecule, which is shown as a stick figure (color code: C atoms, yellow; N atoms, blue; O atoms, red).

compared with vancomycin (Kahne *et al.*, 2005). Recently, new teicoplanin-specific resistance mechanisms have been identified (Novotna *et al.*, 2012), highlighting the urgency of developing new antibacterials that can supersede previous last-resort therapeutics. A detailed molecular understanding of how teicoplanin recognizes its target is likely to aid this development process.

Teicoplanin is secreted from *Actinoplanes teichmyceticus* as a mixture of congeners bearing different fatty-acid substituents. The most abundant congeners are teicoplanins A2-2 and A2-3, which contain branched-chain and straight-chain fatty acids, respectively (Borghi *et al.*, 1984). The fatty-acyl group is thought to anchor the antibiotic to the bacterial membrane, thereby increasing its local concentration at the site of peptidoglycan biosynthesis (Beauregard *et al.*, 1995; Westwell *et al.*, 1996; Cooper *et al.*, 1997). The fatty acid also mediates the formation of higher order oligomers (micelles; Corti *et al.*, 1985; Westwell *et al.*, 1995); this could enhance the binding avidity for the target peptide, which is present in many copies at the bacterial cell surface. The fatty-acyl chain has been shown to be important for antimicrobial activity against VanB-type resistant bacteria, and the entire fatty acyl-glucosamine group is an important contributor to the antimicrobial activity of teicoplanin against enterococci and staphylococci (Liu *et al.*, 2011; Malabarba, Nicas & Ciabatti, 1997; Malabarba, Nicas & Thompson, 1997).

Lipoglycopeptides can prove challenging to crystallize because of the flexibility and low aqueous solubility of the lipid group. Hence, we have chosen to use a carrier-protein strategy for the crystallographic study of teicoplanin in complex with its target peptide (Economou *et al.*, 2012; Moon *et al.*, 2010; Derewenda, 2010; Kobe *et al.*, 1999). We fused the teicoplanin ligand Lys-D-Ala-D-Ala to maltose-binding protein (MBP) or ubiquitin and subsequently crystallized the protein–peptide–antibiotic complex. Here, we describe the resulting structures, which reveal the molecular details of target recognition by teicoplanin. Our structures also show X-ray-induced dechlorination of the antibiotic, which appears to reflect an inherent sensitivity to X-rays on the part of the teicoplanin–target complex.

2. Materials and methods

2.1. Antibiotics and protein constructs

Teicoplanin was purchased from Haorui Pharma-Chem Inc. (Edison, New Jersey, USA) and was used without further purification. The material supplied contained 92% teicoplanin A2-2, with the remainder being made up of other teicoplanin congeners. Vancomycin was purchased from Sigma–Aldrich (St Louis, Missouri, USA). The MBP and ubiquitin carrier-protein constructs were produced as described in Economou *et al.* (2012). Briefly, MBP and ubiquitin were produced in *Escherichia coli* as fusion proteins with a His_6-tagged *Mycobacterium xenopi* intein; the fusion proteins were cleaved in the presence of sodium mercaptoethanesulfonate (MESNA) and subjected to subtractive purification to yield the carrier proteins as C-terminal α-thioesters. These were linked *via* native chemical ligation to a synthetic Cys-Lys-D-Ala-D-Ala peptide. The resulting protein–peptide chimeras were purified prior to crystallization experiments using thiol-Sepharose chromatography to purify the MBP–peptide fusion and anion-exchange chromatography to purify the ubiquitin–peptide fusion. The cysteine side chain was blocked using iodoacetic acid, yielding the *S*-carboxymethyl adduct.

2.2. Crystallization

The Classics, Classics II, PEGs and PEGs II Suites from Qiagen and Additive Screen from Hampton Research were used for initial crystallization screening and optimization. Final optimization of crystallization conditions was performed using hanging-drop vapor diffusion in 24-well plates. All crystallization experiments were carried out at 291 K. The protein–peptide–antibiotic complexes were crystallized using a 1:1.5 molar ratio of protein:antibiotic. The MBP–teicoplanin complex was crystallized using a protein concentration of 10 mg ml^{-1}; the buffer used for the protein–antibiotic complex was 8 m*M* HEPES, 10 m*M* NaCl pH 7 and the reservoir buffer consisted of 0.2 *M* zinc acetate, 0.1 *M* sodium cacodylate pH 6.5, 16% PEG 8000. The ubiquitin–teicoplanin complex was crystallized using a protein concentration of 1.5 mg ml^{-1}; the buffer used for the protein–antibiotic complex was 8 m*M* HEPES, 10 m*M* NaCl pH 7 and the reservoir buffer consisted of 0.1 *M* magnesium chloride, 0.1 *M* sodium acetate pH 4.6, 18% PEG 1500. Prior to data collection, crystals were harvested in nylon loops, treated with cryoprotectant and flash-cooled by plunging them into liquid nitrogen. The cryoprotectants were prepared by mixing three volumes of glycerol with seven volumes of reservoir buffer.

2.3. Structure determination and validation

High-resolution data sets for the MBP–teicoplanin and ubiquitin–teicoplanin complexes were collected on the NE-CAT micro-focus beamline 24-ID of the Advanced Photon Source at Argonne National Laboratory (Table 1). Additional data sets for the MBP–teicoplanin complex were collected on beamlines X25 and X6A of the National Synchrotron Light Source; one of these data sets was collected at the zinc edge to aid in interpreting electron density for ordered solvent atoms and the other was used to estimate the radiation dose. Crystals were maintained at 93 K during data collection. Data were processed using *XDS* (Kabsch, 2010); data-processing statistics are shown in Table 1. Phases were determined by molecular replacement with *MOLREP* (Vagin & Teplyakov, 2010) using the coordinates from PDB entries 1jw4 (Duan & Quiocho, 2002) and 1ubq (Vijay-Kumar *et al.*, 1987) as probes for MBP and ubiquitin, respectively. Structure refinement and model building were carried out using *PHENIX* v.1.6.2-432 (Adams *et al.*, 2010) and *Coot* (Emsley *et al.*, 2010). Refinement statistics are shown in Table 1. The stereochemical library for teicoplanin was generated using *PRODRG* (Schüttelkopf & van Aalten, 2004) and *HIC-Up* (Kleywegt & Jones, 1998). Ramachandran statistics for the proteins were

Table 1
Data-collection and refinement statistics.

Values in parentheses are for the highest resolution shell.

Complex	MBP-peptide fusion + teicoplanin (PDB entry 3vfj)	Ubiquitin-peptide fusion + teicoplanin (PDB entry 3vfk)	MBP-peptide fusion + teicoplanin, zinc edge	MBP-peptide fusion + teicoplanin, crystal-irradiation experiment
Data collection				
Beamline	NE-CAT 24-ID, APS	NE-CAT 24-ID, APS	NSLS X25	NSLS X6A
X-ray wavelength (Å)	0.9792	0.9792	1.283	0.9794
Space group	$C222_1$	$C2$	$C222_1$	$C222_1$
Unit-cell parameters (Å)				
a	40.67	88.01	40.32	40.63
b	123.84	25.18	123.61	124.01
c	156.49	38.71	156.74	156.18
Resolution range (Å)	39.89–2.05 (2.12–2.05)	19.29–2.80 (2.90–2.80)	19.95–2.20 (2.26–2.20)	19.66–2.00 (2.05–2.00)
No. of observations	267153 (19103)	10018 (1021)	282744 (18967)	131839 (9080)
No. of unique reflections	47482 (3534)	2084 (208)	38407 (2846)	50590 (3834)
$\langle I/\sigma(I)\rangle$	10.89 (2.78)	8.11 (2.38)	15.86 (2.95)	13.16 (2.19)
Completeness (%)	100 (99.9)	99.2 (99.0)	99.8 (99.7)	98.1 (98.1)
Average multiplicity	5.6 (5.4)	4.8 (4.9)	7.4 (6.7)	2.6 (2.36)
$R_{\rm merge}$†	0.10 (0.71)	0.14 (0.65)	0.13 (0.73)	0.05 (0.41)
$R_{\rm meas}$‡	0.11 (0.79)	0.14 (0.69)	0.14 (0.80)	0.07 (0.52)
Refinement				
$R/R_{\rm free}$§	0.189/0.231	0.271/0.310		0.199/0.240
Wilson B factor (Å^2)	31.6	70.2		27.3
Average B factor (Å^2)				
Protein	31.3	69.9		29.04
Water	33.8	60.1		33.11
Antibiotic	34.4	72.6		30.41
No. of protein atoms	2902	627		2904
No. of antibiotic atoms	131	131		131
No. of water molecules	155	15		177
R.m.s. deviation from ideality¶				
Bond lengths (Å)	0.006	0.005		0.005
Bond angles (°)	1.05	0.82		1.04
Protein geometry††				
Ramachandran plot (%)				
Outliers	0.0	0.0		0
Favored	99.0	97.7		99.0
Allowed	1.0	2.3		1.0
Clashscores	11.2	23.5		—
C^β deviations > 0.25 Å	0.0	0.0		0.0
Poor rotamers	0.0	0.0		0.34

† $R_{\rm merge}$ is calculated as $R_{\rm merge} = \sum_{hkl}\sum_i |I_i(hkl) - \langle I(hkl)\rangle| / \sum_{hkl}\sum_i I_i(hkl)$, where $I_i(hkl)$ is the ith measurement of the intensity of reflection hkl. ‡ $R_{\rm meas}$ (or redundancy-independent $R_{\rm merge}$) is calculated as $R_{\rm meas} = \sum_{hkl}\{N(hkl)/[N(hkl)-1]\}^{1/2}\sum_i |I_i(hkl) - \langle I(hkl)\rangle| / \sum_{hkl}\sum_i I_i(hkl)$, where $I_i(hkl)$ is the ith measurement and $N(hkl)$ is the redundancy of the unique reflection hkl. § $R_{\rm free}$ is calculated using 5% of the reflections chosen at random and omitted from refinement; $R_{\rm work}$ is calculated using the remaining 95% of the reflections. ¶ Ideal values taken from Engh & Huber (1991) as implemented in *PHENIX* v.1.6.2-432 (Adams *et al.*, 2010). †† The *MolProbity* server was used for validation (Chen *et al.*, 2010).

calculated with *MolProbity* (Chen *et al.*, 2010). Structure figures were generated using *PyMOL* v.0.99.rc6 (DeLano, 2002). The final electron-density maps are shown in Supplementary Fig. S7[1]. Coordinates and structure factors have been deposited in the Protein Data Bank with accession codes 3vfj (MBP–teicoplanin) and 3vfk (ubiquitin–teicoplanin).

2.4. Surface plasmon resonance

Binding constants were measured using surface plasmon resonance as described in Economou *et al.* (2012). Briefly, carrier protein-peptide fusions were immobilized on ProteOn GLC sensor chips (Bio-Rad, Hercules, California, USA) using a mixture of 1-ethyl-3-(3-dimethylaminopropyl carbodiimide hydrochloride) and sulfo-*N*-hydroxysuccinimide. The unfused thioester form of MBP-Ala_5 and the ubiquitin D77 mutant were included as control surfaces. Excess active ester groups on the sensor surface were capped with ethanolamine–HCl pH 8.5. The unfused peptide Cys-Lys-D-Ala-D-Ala was immobilized on ProteOn GLH sensor chips pre-activated with a mixture of 1-ethyl-3-(3-dimethylaminopropyl carbodiimide hydrochloride) and sulfo-*N*-hydroxysuccinimide and then treated with 3,3′-*N*-(ε-maleimidocaproic acid) hydrazide (trifluoroacetic acid salt; Thermo Scientific). Excess maleimide groups were blocked with cysteine. A scrambled peptide (Cys-L-Ala-Lys-L-Ala) was used as a control surface. Teicoplanin was injected over the control and target ligand surfaces at a flow rate of 100 µl min^{-1} for a 2 min association phase followed by a 3–10 min dissociation phase at 298 K using the 'one-shot kinetics' functionality of the ProteOn (Bravman *et al.*, 2006). Data were analyzed using the *ProteOn Manager*

[1] Supplementary material has been deposited in the IUCr electronic archive (Reference: KW5054). Services for accessing this material are described at the back of the journal.

Table 2
Data subsets used in the crystal-irradiation experiments.

Rotation angle	0–90°	0–125°	35–125°
No. of observations	94550 (5967)	131839 (9080)	96816 (6583)
No. of unique reflections	49689 (3352)	50590 (3834)	40360 (3050)
$\langle I/\sigma(I)\rangle$	12.1 (2.0)	13.2 (2.2)	12.5 (2.1)
Completeness (%)	96.3 (87.1)	98.1 (98.1)	78.1 (79.4)
$R_{\rm merge}$	0.045 (0.376)	0.052 (0.410)	0.050 (0.389)
$R_{\rm meas}$	0.061 (0.513)	0.065 (0.522)	0.062 (0.492)

software v.3.0. The responses of buffer injections and responses from the reference flow cell were subtracted to account for injection artifacts and nonspecific binding. Equilibrium dissociation constants ($K_{\rm d}$) were obtained by fitting equilibrium-binding data in the *ProteOn Manager* software using the four-parameter equation

$$\text{Response} = R_{\rm high} + \frac{(R_{\rm high} - R_{\rm low})}{1 + \left(\dfrac{\text{Conc}}{A_1}\right)^{A_2}},$$

where $R_{\rm high}$ is the response value at high analyte concentrations, $R_{\rm low}$ is the response at zero analyte concentrations, A_1 is the mid-range concentration and is equivalent to the equilibrium constant ($K_{\rm d}$) and A_2 is the slope factor. Binding curves and representative SPR sensorgrams are shown in Supplementary Figs. S1 and S2.

2.5. Irradiation experiments

For the crystal-irradiation experiments, a 125° data set was collected using a beam size of 150 × 150 µm (Tables 1 and 2). The crystal dimensions were 200 × 30 × 40 µm. The flux was calculated as described in Owen *et al.* (2009) for a 51 µm thick silicon photodiode with a 6 µm thick aluminium filter, and the absorbed dose was calculated using *RADDOSE* (Paithankar *et al.*, 2009). The structure was refined against the full 125° data set using *PHENIX* as described in §2.3, assuming full occupancy for both Cl atoms. Data-collection and refinement statistics are shown in Table 1. For analysis of dechlorination, the data set was divided into subsets as described in §3, which were used to calculate $2F_{\rm o} - F_{\rm c}$ and $F_{\rm o} - F_{\rm c}$ maps.

For solution-irradiation experiments, teicoplanin, teicoplanin plus peptide (acetyl-Lys-D-Ala-D-Ala; Sigma–Aldrich, St Louis, Missouri, USA) or vancomycin plus peptide were dissolved in 20 m*M* HEPES pH 7.5, 5 m*M* EDTA, 17% DMSO with final antibiotic concentrations of 23 m*M*. Approximately 1.5 µl of each sample was dispensed into a 1 mm diameter glass capillary (Charles Supper Company, Natick, Massachusetts, USA). Samples were irradiated on NSLS beamline X6A at room temperature, rotating at 4° per second, using a beam energy of 11 500 eV; the beam size was approximately 0.7 × 0.5 mm (horizontal × vertical). After exposure, each sample was removed from the capillary, transferred into a PCR tube and stored in liquid nitrogen. Samples were analyzed at the Washington University Mass Spectrometry Resource (St Louis, Missouri, USA) using a Thermo Finnigan LTQ-FT mass spectrophotometer with electrospray ionization; the spectrum was acquired over an m/z range of 150–2000 Da. Because of various experimental constraints militating against accurate estimates (*e.g.* samples larger than the beam, significant variation in capillary diameter, bubble formation *etc.*), no effort was made to calculate the exact dose received by each sample.

3. Results

3.1. Carrier-protein strategy

Teicoplanin is a 'large small molecule'; *i.e.* although smaller than biological macromolecules such as proteins, it is large by the standards of small-molecule crystallography and hence not well suited for classical direct methods of phase determination. Modern dual-space direct methods have enjoyed excellent success with molecules such as teicoplanin (Usón & Sheldrick, 1999), but require near-atomic resolution diffraction data to ensure success (Morris & Bricogne, 2003; Sheldrick, 1990). Such resolution requires very well ordered crystals, which are sometimes difficult to obtain, particularly when the molecule of interest contains potential sources of conformational heterogeneity such as sugars and lipids, as does teicoplanin. The lipid group also reduces the aqueous solubility of teicoplanin, complicating crystallization.

To avoid potential problems in both crystallization and phasing, we chose to use a carrier-protein strategy to study the complex of teicoplanin with its cell-wall target peptide. This approach has been used in a variety of systems in the past two decades (Moon *et al.*, 2010; Derewenda, 2010; Kobe *et al.*, 1999; Koide, 2009) and has recently been shown to be valuable for the structural analysis of other glycopeptide antibiotics (Economou *et al.*, 2012). Here, we covalently linked the teicoplanin ligand (Lys-D-Ala-D-Ala) to a carrier protein *via* native chemical ligation (Evans *et al.*, 1998; Muir, 2003). Subsequently, we cocrystallized the antibiotic with the carrier protein–peptide fusion. The carrier protein improved the solubility of the antibiotic target complex and provided additional surface area for crystal lattice contacts; it also greatly simplified structure determination by allowing us to perform molecular replacement using the known structure of the carrier protein as a probe.

The protein carrier initially selected was the *E. coli* maltose-binding protein (MBP) because it is highly soluble and readily crystallized and because its structure is known. It also adopts two different stable conformations in the presence and in the absence of maltose (Duan & Quiocho, 2002); these two conformations promote different crystal contacts, thus increasing the possibility of crystallization of the complex of interest. To ensure that the carrier protein did not block access to the Lys-D-Ala-D-Ala target peptide, we inserted a five-alanine linker between the C-terminus of MBP and the target peptide. To confirm that the presence of the carrier protein did not interfere with recognition of the target peptide by the antibiotic, we measured the binding of teicoplanin to the carrier protein–peptide fusion using surface plasmon resonance (Supplementary Fig. S1). The binding affinity ($K_{\rm d}$) of

teicoplanin for the carrier protein–peptide fusion was found to be 91 ± 7 n*M*, which is in good agreement with the values previously measured for the free Lys-D-Ala-D-Ala peptide, which range from 40 to 630 n*M* (Malabarba, Trani *et al.*, 1989; Scrimin *et al.*, 1996; Cooper *et al.*, 1997; Arriaga *et al.*, 1990). In the same surface plasmon resonance assay, the K_d value for the peptide alone (without carrier protein) was found to be 474 ± 20 n*M*, which is also in agreement with previous results (Supplementary Fig. S2). Thus, the presence of the MBP carrier protein does not interfere with teicoplanin's recognition of its ligand.

Crystallization conditions for the complex of teicoplanin with the MBP-Ala_5-peptide fusion were readily identified using commercially available screening kits. We obtained well diffracting crystals in the absence of maltose in a condition similar to one previously reported (Center *et al.*, 1998). Structure determination by molecular replacement was straightforward using the known MBP structure. Maps calculated using phases from the molecular-replacement model showed clear electron density corresponding to teicoplanin bound to the Lys-D-Ala-D-Ala peptide at the C-terminus of the MBP molecule.

3.2. Description of the teicoplanin structure

Teicoplanin adopts a curved conformation, with the N- and C-termini of the antibiotic closing around the target peptide to form a concave binding pocket (Fig. 1). The mannose attached to amino acid 7 at the C-terminal end of the antibiotic interacts with a hydroxyl group on the side chain of amino acid 1 at the N-terminal end of the molecule, forming a hydrogen bond (3.1 Å); the side chains of amino acids 1 and 7, together with the mannose, form the floor of the ligand-binding pocket. A similar closure of the antibiotic molecule around its ligand is seen in the other group III glycopeptide antibiotics ristocetin and dalbavancin (Nahoum *et al.*, 2009; Economou *et al.*, 2012). The peptide backbone, together with the side chains of residues 2, 4 and 6, form the rear of the binding pocket. The top of the binding pocket is formed by the glucosamine sugar attached to the side chain of residue 4, which projects outward over the concave binding pocket. The fatty-acyl chain attached to the glucosamine lies on the back (convex) face of the antibiotic. This positioning of the acyl chain sterically prevents teicoplanin from forming the types of back-to-back dimers that are observed with many other glycopeptide antibiotics (Waltho & Williams, 1989; Sheldrick *et al.*, 1995; Loll *et al.*, 1997; Schäfer *et al.*, 1996). An additional sugar moiety, an *N*-acetylglucosamine attached to amino acid 6, contributes steric bulk that may also contribute to blocking back-to-back dimer formation.

3.3. Teicoplanin ligand binding

Teicoplanin embraces its Lys-D-Ala-D-Ala target within its concave binding pocket, with the peptide backbones of the ligand and antibiotic aligning in an antiparallel manner. Five hydrogen bonds connect the ligand to the peptide backbone of the antibiotic (Fig. 2*a*) and involve interactions between the following pairs of atoms: the backbone amide N atom of teicoplanin residue 2 and one carboxylic acid O atom of the peptide target (2.8 Å), the backbone amide N atoms of teicoplanin residues 3 and 4 and the other O atom of the carboxylate group of the ligand (2.9 and 2.8 Å, respectively), the carbonyl O atom of teicoplanin amino acid 4 and the backbone amide N atom of the C-terminal D-Ala of the target (2.9 Å), and the backbone amide N atom of teicoplanin residue 7 and the carbonyl O atom of the lysine residue of the peptide (3.0 Å). These are the same five hydrogen bonds used for target recognition by vancomycin and other glycopeptide antibiotics (Kalman & Williams, 1980; Loll & Axelsen, 2000).

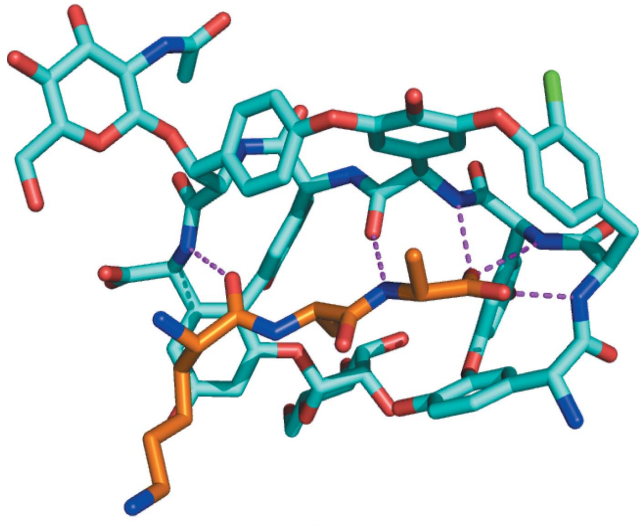

(*a*)

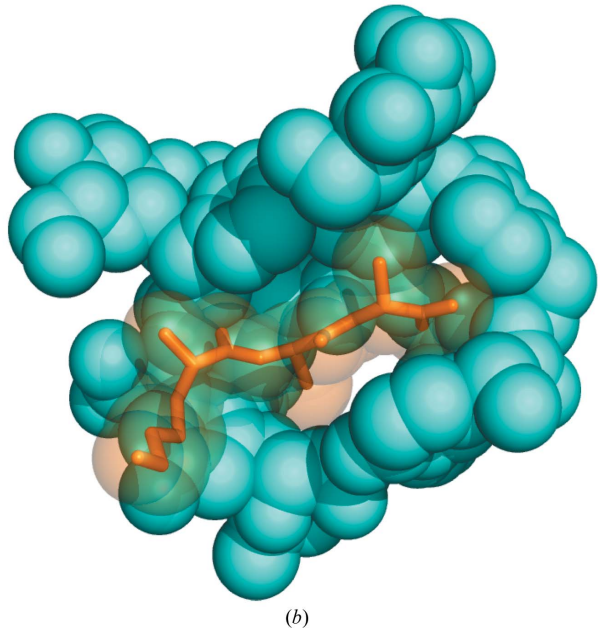

(*b*)

Figure 2
Interactions of teicoplanin with its ligand. (*a*) Teicoplanin recognizes its target *via* five hydrogen bonds (dashed magenta lines) that connect the peptide backbone of the antibiotic to the ligand. For clarity, the *N*-acylglucosamine attached to amino acid 4 is omitted from this view. (*b*) Teicoplanin wraps around its ligand. Teicoplanin (cyan) is shown in a sphere representation and its peptide ligand (orange) is shown in a stick representation with transparent spheres overlaid.

In addition to forming these hydrogen bonds, teicoplanin wraps around its ligand, shielding it from solvent. The interior face of the binding pocket, formed by the side chains of teicoplanin residues 2, 4 and 6, shields one face of the peptide ligand; the side chain of residue 1 partially shields the opposite face of the C-terminal portion of the ligand. A similar tight embrace has been observed with the related glycopeptide antibiotics ristocetin and dalbavancin (Nahoum *et al.*, 2009; Economou *et al.*, 2012). In the teicoplanin structure additional shielding is provided by the glucosamine sugar attached to amino acid 4 of the antibiotic, the C5 atom of which makes a van der Waals contact with the side chain of the C-terminal D-Ala residue of the ligand (Fig. 2*b*). In addition to the conformation it adopts in our structure, this sugar is capable of adopting a conformation that is rotated by approximately 180° (Westwell *et al.*, 1995; Heald *et al.*, 1987); however, this rotation would place the fatty-acyl group over the binding site and interfere with ligand binding.

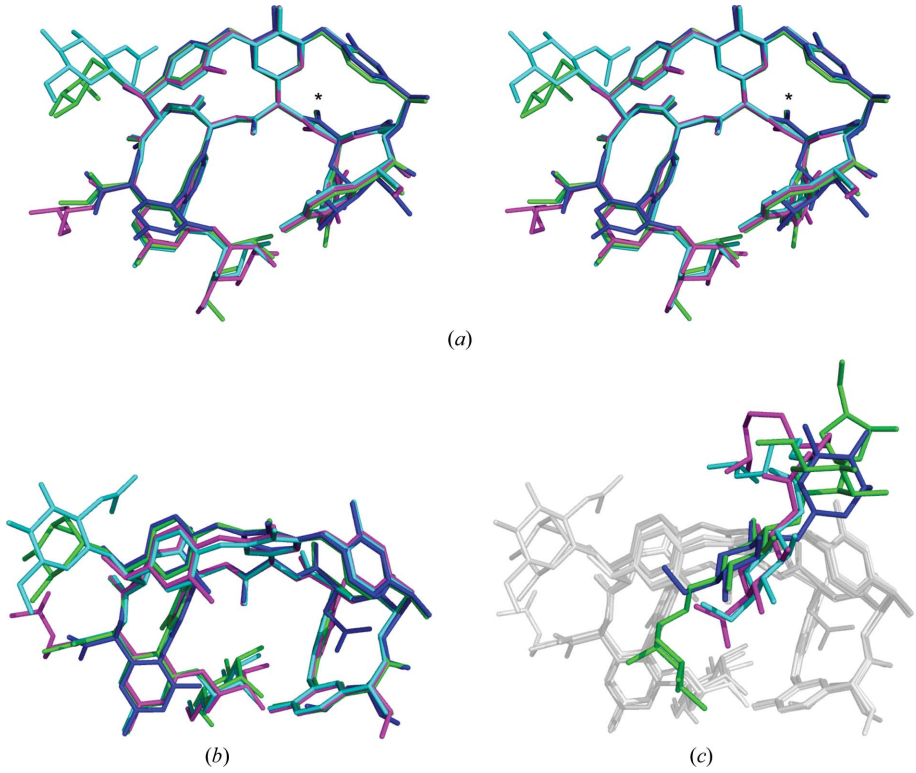

Figure 3
Structural comparison of teicoplanin with other glycopeptide antibiotics. (*a*) Stereo representation of the C^{α} superposition of teicoplanin (cyan), dalbavancin (magenta), ristocetin (green) and vancomycin (blue). The position of the carbonyl group on residue 3 is marked with an asterisk. Substituents attached to amino acid 4 are omitted for the sake of clarity. (*b*) The same as (*a*) but tilted towards the viewer by approximately 20°. (*c*) The same as (*b*) but showing the various substituents on amino acid 4. The color code for the substituents is the same as in (*a*).

The N-terminal portion of the target peptide contributes little, if anything, to antibiotic target recognition. The side chain of the lysine residue does not interact with the antibiotic, nor does any portion of the peptide chain upstream of this residue.

3.4. Structural comparison of teicoplanin with other glycopeptides

The chemical structure of teicoplanin resembles that of dalbavancin (Malabarba & Goldstein, 2005), a semi-synthetic antibiotic that is currently in clinical trials. Although dalbavancin lacks a sugar group on amino acid 6, like teicoplanin it carries a chlorine on amino acid 6 and a sugar with an attached fatty-acyl group on amino acid 4. Also, neither teicoplanin nor dalbavancin form back-to-back dimers, distinguishing them from many other glycopeptide antibiotics (Beauregard *et al.*, 1995; Colombo *et al.*, 2009). As might be expected from the high degree of similarity between the two molecules, teicoplanin superposes almost perfectly with dalbavancin (Economou *et al.*, 2012), with an r.m.s. difference in backbone C^{α} positions of 0.11 Å (Fig. 3). After superposition of the backbone atoms, the side chains of all amino acids of the two antibiotics also overlay each other closely.

The sugar and fatty-acyl moieties attached to the fourth amino acids of teicoplanin and dalbavancin are similar but not identical; teicoplanin carries an *N*-acylglucosamine while dalbavancin carries an *N*-acylaminoglucuronic acid, and the acyl group of teicoplanin is one carbon shorter than that of dalbavancin. Nevertheless, the sugar moieties in the two structures superpose very well, lying over the center of the ligand-binding site, where they both form van der Waals interactions with their respective bound ligands. This places the fatty-acyl chains of both molecules on the back of the glycopeptide, *i.e.* on the face opposite the ligand-binding site. The fatty-acyl groups of teicoplanin and dalbavancin occupy approximately the same position but have different conformations, very likely reflecting high intrinsic flexibility (Economou *et al.*, 2012).

Teicoplanin is less chemically similar to vancomycin and ristocetin than it is to dalbavancin. Ristocetin, which like teicoplanin is a group III glycopeptide antibiotic, contains linked aromatic side chains for amino acids 1 and 3; however, ristocetin contains no Cl atoms and possesses a tetrasaccharide substituent attached to amino acid 4, as opposed to the fatty-acylated monosaccharide in teicoplanin. Vancomycin is even less similar to teicoplanin than ristocetin is, containing unlinked non-aromatic residues at positions 1 and 3 and no mannose substituent on amino acid 7. Despite these differences, both ristocetin and vancomycin superpose on the teicoplanin structure reasonably well, with r.m.s. differences in C^{α} positions of 0.17 and 0.34 Å, respectively. However, several significant differences emerge from this comparison. Firstly, for vancomycin the lack of a mannose substituent at amino

acid 7 allows the N- and C-termini of the antibiotic to approach each other more closely than is observed for the other drugs, permitting the antibiotic to adopt a slightly more pronounced curvature (Fig. 3). Secondly, the backbone carbonyl O atom of amino acid 3 assumes a different orientation in teicoplanin and dalbavancin than it does in ristocetin and vancomycin (Economou *et al.*, 2012). In ristocetin and vancomycin this oxygen hydrogen bonds to an amide N atom on another antibiotic monomer, helping to form the back-to-back dimer (Waltho & Williams, 1989; Sheldrick *et al.*, 1995). Teicoplanin does not form such dimers and its structure reveals that in the absence of this hydrogen bond the antibiotic backbone is able to relax its position slightly at amino acid 3 (Fig. 3).

Another difference between dimer-forming and non-dimer-forming antibiotics is a small but significant 'twist' exhibited by the side chains of residues 4 and 6. In dimer-forming antibiotics, as compared with non-dimer-forming molecules, these side chains move towards the back of the molecule with respect to the backbone position (Fig. 3). This difference can be explained by σ–π interactions between aromatic groups across the dimer interface which draw the side chains of amino acids 4 and 6 backwards, away from the ligand-binding pocket. This conformational twist affects the position of the substituents bound to amino acid 4. Thus, in teicoplanin and dalbavancin the sugars attached to amino acid 4 are centered directly over the ligand-binding site, whereas the sugars attached to the corresponding positions of ristocetin and vancomycin are offset from the ligand-binding pocket and moved toward amino acid 6. This offset is accentuated by the steric effects associated with the presence of two copies of the sugar substituents in an antibiotic dimer. Hence, in the monomeric antibiotics the sugar moieties are more free to move to adjust their position with respect to that of the ligand, whereas in dimeric antibiotics they are considerably more constrained.

The structure reported here is to our knowledge the first crystal structure of teicoplanin bound to its peptide ligand. However, other structures are available for teicoplanin or its derivatives bound to various enzymes implicated in glycopeptide antibiotic biosynthesis. These enzymes include the sulfotransferase Teg12 (Bick *et al.*, 2010; PDB entries 3mg9 and 3mgb) and the deacetylase Orf2 (Chan *et al.*, 2011; PDB entry 2xad)[2]. Two copies each of the teicoplanin aglycon are found in 3mg9 and 3mgb; three of these four molecules adopt configurations similar to that seen in the structure reported here (r.m.s. difference in C^{α} positions of 0.36–0.49 Å; see Fig. 4*a*). In contrast, there are marked differences between the fourth teicoplanin molecule (found in 3mgb) and our structure (r.m.s. difference in the C^{α} positions of 1.77 Å; see Fig. 4*b*). The N-terminus of this fourth teicoplanin molecule is in an open configuration: the carbonyl group of amino acid 3 is flipped and points towards the ligand-binding site, and there is an attendant movement of the side chain of residue 1 away from the binding pocket. In 2xad the asymmetric unit contains four copies of the teicoplanin molecule which all adopt

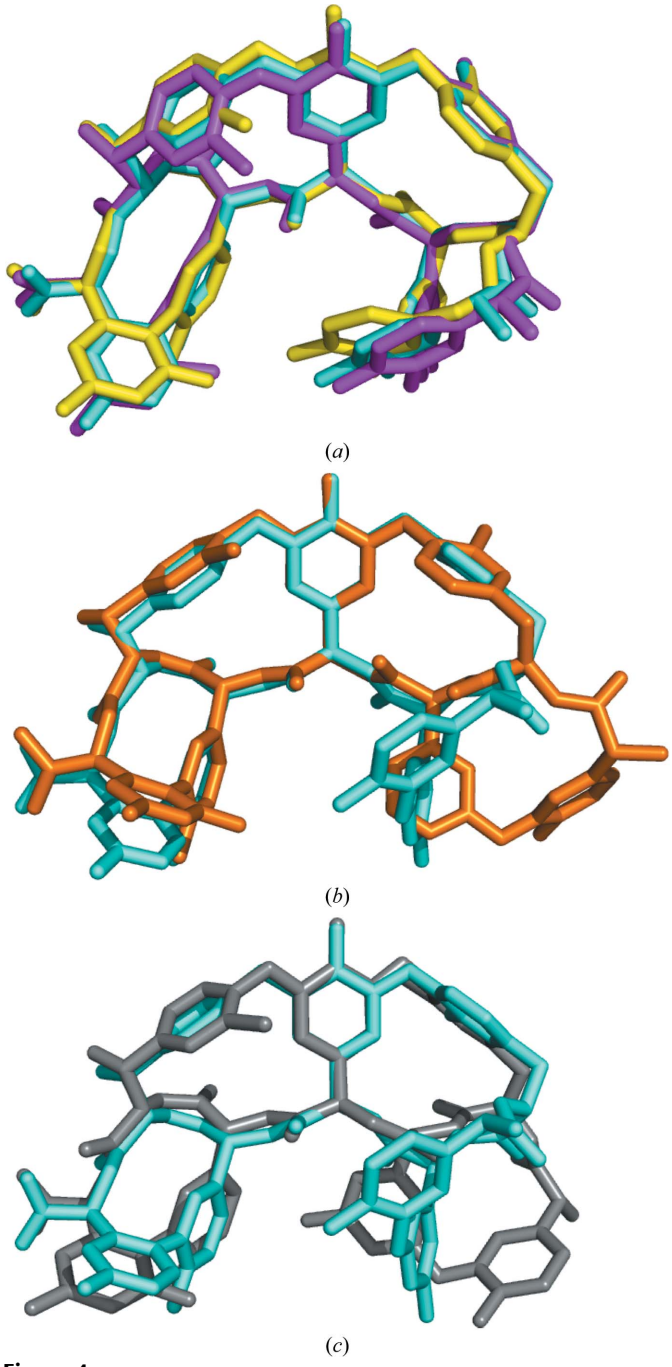

Figure 4
Flexibility in the teicoplanin backbone. (*a*) Superposition of our teicoplanin structure (cyan) with two representative structures of similar teicoplanin conformers bound to the Teg12 sulfotransferase (magenta and yellow; derived from PDB entries 3mgb and 3mg9, respectively; Bick *et al.*, 2010). (*b*) Superposition of our teicoplanin structure (cyan) with that of teicoplanin in complex with the Orf2 deacetylase (orange; PDB entry 2xad; Chan *et al.*, 2011). (*c*) Superposition of our teicoplanin structure (cyan) with that of the dissimilar teicoplanin conformer bound to the Teg12 sulfotransferase (gray; PDB entry 3mgb; Bick *et al.*, 2010). Only the aglycon portions of the teicoplanin molecules are shown.

[2] Another teicoplanin structure has been reported for a putative complex of the antibiotic with the hexose oxidase Dbv29 (Liu *et al.*, 2011; PDB entry 2wdx). However, when we calculated electron-density maps for this structure using the deposited structure factors we saw no convincing density for the teicoplanin molecule; thus we have not included it in our analysis.

similarly open N-terminal configurations (the r.m.s. differences in teicoplanin C^{α} positions between our structure and those in 2xad range from 1.61 to 1.67 Å; see Fig. 4*b*). Furthermore, in the 2xad structure two of the four teicoplanin molecules also have the carbonyl group of residue 2 flipped to face the ligand-binding site in addition to the carbonyl group of amino acid 3. These peptide flips serve to move the side chain of residue 1 away from the ligand-binding site and the side chain of amino acid 2 towards the ligand-binding site. The combined effect of these changes is to drastically alter the conformation of the first three residues of teicoplanin (Figs. 4*b* and 4*c*), thereby abolishing the ligand-binding pocket.

Multiple possible conformations for the backbone of teicoplanin have previously been suggested based on NMR solution studies (Heald *et al.*, 1987). One of the conformations suggested in this earlier work resembles our ligand-bound conformation; details of the other conformation could not be fully determined with the NMR data available at the time, but may correspond to the open conformation seen in the 2xad and 3mgb structures. A parameter that appears to correlate with this open/closed conformational switch is the occupancy of the ligand-binding site. In our structure, which adopts a closed conformation, the binding site is occupied by the cell-wall peptide. In 3mg9, which also shows a normal closed binding-site architecture, the binding sites of the two teicoplanin molecules in the asymmetric unit are occupied by either a glutamate side chain of the enzyme or a glycerol molecule, each of which makes interactions with the teicoplanin that mimic those made by the C-terminus of the natural ligand. In contrast, no ligand occupies the binding site in 2xad, in which all four molecules in the asymmetric unit show open-conformation binding sites, or in 3mgb, in which one of two molecules in the asymmetric unit has an open binding site. Thus, while glycopeptide antibiotics have generally been thought to be rigid molecules, it appears that in the case of teicoplanin formation of the binding pocket is a dynamic process that is controlled (at least in part) by the presence of the ligand.

3.5. Dechlorination of teicoplanin

Teicoplanin contains two covalently bound Cl atoms, one in each of the 3-chlorophenylglycine residues found at positions 4 and 6 in the sequence (Fig. 1). However, we did not detect electron density corresponding to the Cl atom of residue 6 during refinement, instead observing a negative peak at this position in $F_o - F_c$ maps (Fig. 5). Mass-spectrometric analysis confirmed that our starting material had the correct mass for the dichloro species (Supplementary Fig. S3), indicating that the chlorine was lost either during crystallization or during the X-ray diffraction experiment. To determine whether the chlorine was removed during crystallization, we washed crystals of the MBP–peptide–teicoplanin complex in protein-free and teicoplanin-free buffer, dissolved them and compared their mass spectrum with that of uncrystallized teicoplanin (Supplementary Fig. S3). The spectra showed no indication of dehalogenation in the crystals, indicating instead that loss of the Cl atom occurs upon X-ray exposure.

In order to assess the dose-dependence of dehalogenation, we measured a data set from a crystal of the teicoplanin–MBP–peptide complex (labeled 'crystal-irradiation experiment' in Table 1); we then used *RADDOSE* to estimate the absorbed dose (Paithankar *et al.*, 2009). We exposed the crystal for a total rotation angle of 125°; analysis of these data showed that the minimum rotation angle for which a reasonably complete data set could be assembled was ∼90°. We then calculated electron-density maps using three different subsets of the data (Table 2). The first data set included only the first 90° of rotation, which corresponds to an absorbed dose of 3.6 MGy. The second data set included the entire 125° swath, corresponding to a dose of 5.0 MGy. The third data set included only the final 90° of rotation, which we reasoned would be the most affected by radiation damage. Even for the first 90°, we saw no electron density for the Cl atom of amino acid 6 (Fig. 5), indicating that this chlorine was lost relatively

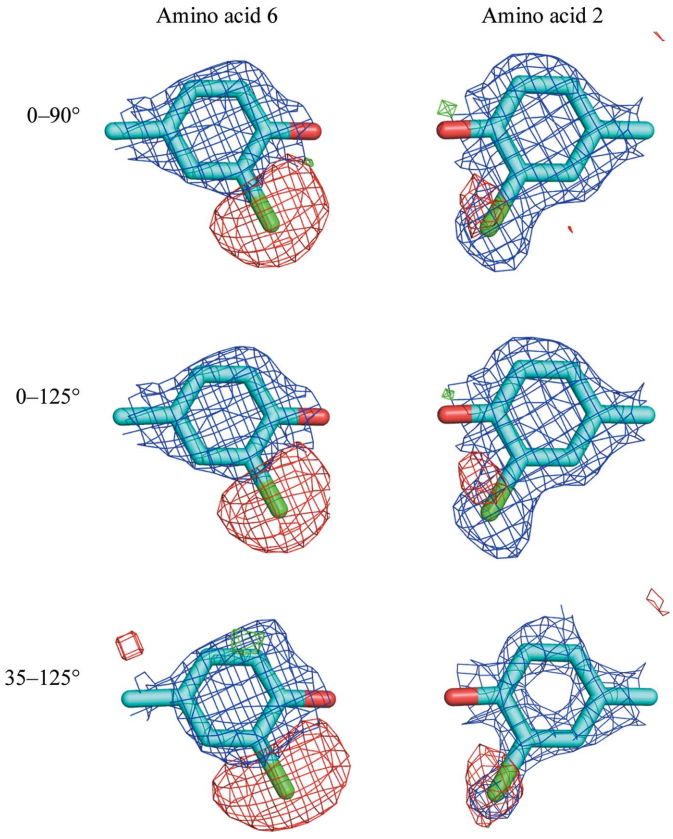

Figure 5
Dechlorination of teicoplanin upon X-ray exposure. A crystal of teicoplanin bound to the MBP-Ala_5-peptide fusion was irradiated over a total rotation angle of 125° and the data were divided into three subsets as described in Table 2. For each data set, $F_o - F_c$ maps were calculated using a model that contains a chlorine on amino acid 6 to calculate F_c values; these maps are shown contoured at $\pm 3.0\sigma$ (red, negative; green, positive). $2F_o - F_c$ OMIT maps were also calculated, for which the Cl atoms on both residues 2 and 6 were omitted from the structure-factor calculation. These maps are shown in blue contoured at 1.0σ. The teicoplanin model is illustrated in a stick representation, with C atoms colored cyan, O atoms red and Cl atoms green.

rapidly. In contrast, the Cl atom on amino acid 2 is present at essentially full occupancy in these maps. Over time, however, the occupancy of this chlorine decreases as well; negative difference density appears around this atom in the $F_o - F_c$ map for the full 125° data set and becomes more pronounced in the map calculated using the final 90° of data (Fig. 5). Nonetheless, even under conditions of maximum damage this chlorine position appears to be at least partially occupied. Therefore, we conclude that X-ray exposure of the MBP–teicoplanin crystals leads to a rapid dechlorination event at amino acid 6 of teicoplanin, as well as slower dechlorination at amino acid 2.

3.5.1. Generality of the dechlorination phenomenon. It seemed unlikely that the MBP carrier protein was contributing to the dechlorination of teicoplanin; however, our previous experience with this carrier protein was limited to the crystallization of ristocetin (Economou *et al.*, 2012), and since ristocetin contains no halogen atoms we could not rigorously rule out the possibility that MBP might be influencing the dehalogenation process. To confirm that teicoplanin dechlorination was not being induced by the presence of MBP, we crystallized the teicoplanin–ligand complex using a different carrier protein, ubiquitin. This carrier protein was previously used to crystallize dalbavancin, a glycopeptide antibiotic that carries a chlorine on amino acid 6 and for which no dechlorination was observed (Economou *et al.*, 2012). In our SPR assay teicoplanin recognized the ubiquitin target peptide complex with a K_d value of 191 ± 14 n*M*, similar to the values obtained with the MBP fusion and the peptide alone.

Using ubiquitin as a carrier protein, we obtained crystals of the teicoplanin–ligand complex that diffracted to 2.8 Å resolution. We determined the structure by molecular replacement using the known structure of ubiquitin as a probe (Table 1 and Supplementary Figs. S4 and S5). We then carried out refinement and examined the chlorine occupancy. As was the case with the MBP complex, no electron density was observed for the chlorine on amino acid 6 (Supplementary Fig. S6). Density was observed for the chlorine on amino acid 2, but difference maps showed negative density for this atom, indicating partial dehalogenation at this site, similar to what was observed with MBP. Thus, teicoplanin dechlorination is not caused by a specific carrier protein; instead, it appears that teicoplanin itself is intrinsically sensitive to X-rays.

3.5.2. Irradiation studies in solution. To test the intrinsic sensitivity of teicoplanin to X-rays outside a crystal environment, we irradiated concentrated room-temperature solutions of both teicoplanin and vancomycin in the presence or absence of stoichiometric amounts of the peptide ligand acetyl-Lys-D-Ala-D-Ala. After irradiation, we flash-cooled the samples and subsequently analysed them using mass spectrometry (Fig. 6). We observed that for teicoplanin dehalogenation proceeded relatively slowly in the absence of ligand. The peptide-free sample showed about 15% conversion to the monochloro form after 15 min of irradiation; longer irradiation times led to an increase in the relative amount of the monochloro species plus an overall loss of signal that presumably corresponds to global radiation damage (Fig. 6). In contrast, after 15 min the peptide plus ligand sample contained approximately 40% of the monochloro species; more significantly, however, this level of irradiation led to a massive loss of signal compared with the ligand-free sample, indicating a much higher overall level of radiation damage. Thus, teicoplanin appears to become significantly more sensitive to X-ray-induced damage in the presence of its ligand. This radiosensitization is not a general phenomenon associated with the presence of the ligand, because in the presence of the same ligand vancomycin exhibited dehalogenation kinetics that were roughly comparable to those observed for ligand-free teicoplanin.

4. Discussion

Teicoplanin is a clinically important glycopeptide antibiotic used to treat life-threatening infections caused by multi-drug-resistant bacterial pathogens. It inhibits the formation of the bacterial cell wall by binding and sequestering D-Ala-containing peptides in cell-wall precursors. Here, we report the first crystal structure of a complex of teicoplanin with a cell-wall peptide, obtained using a carrier-protein strategy. The presence of the carrier protein assists at both the level of crystallization (by contributing additional rigid surface area for crystal packing) and at the level of phase determination (in this case by molecular replacement, but anomalous dispersion approaches using selenomethionine could also be used).

This new structure, in combination with previous ligand-free structures, reveals a hitherto unsuspected degree of structural plasticity in the heptapeptide core of teicoplanin which allows the N-terminal portion of the molecule to undergo a large conformational change in the absence of ligand (Fig. 4). This change involves several peptide flips and opens and flattens the normally concave ligand-binding pocket. No similar open conformation has been described for any other glycopeptide antibiotics. Interactions between the antibiotic and its ligand (notably, hydrogen bonds between the backbone of the antibiotic and the terminal carboxylate of the ligand) appear to be sufficient to pull the molecule into its more closed concave conformation.

By using two different carrier proteins, we have captured teicoplanin in two different crystalline environments. In the MBP structure the back face of the antibiotic packs against an MBP molecule in an adjacent asymmetric unit at the opening of the maltose-binding site of the protein. The antibiotic makes extensive interactions with this neighboring protein molecule, including hydrophobic interactions between the fatty-acyl chain of the antibiotic and the aromatic side chains of the protein and hydrogen bonds and van der Waals interactions between the sugars of the antibiotic and the peptide backbone and side chains of the protein. However, despite these extensive interactions within the maltose-binding site of the protein, MBP remains in its maltose-free conformation (Duan & Quiocho, 2002). In the ubiquitin–teicoplanin structure only a few weak hydrogen bonds contribute to lattice packing; in the principal packing interaction involving teicoplanin the back of the teicoplanin heptapeptide interacts with

an adjacent ubiquitin molecule in the crystal lattice *via* the so-called 'Ile44 patch', a small hydrophobic patch on the ubiquitin surface. Teicoplanin adopts similar conformations in both crystal forms (Supplementary Fig. S5), with an r.m.s. difference in C^{α} positions of 0.30 Å. The resolution of the ubiquitin structure is substantially lower than that of the MBP structure, so the significance of minor antibiotic structural differences between the two crystal forms is unclear; however,

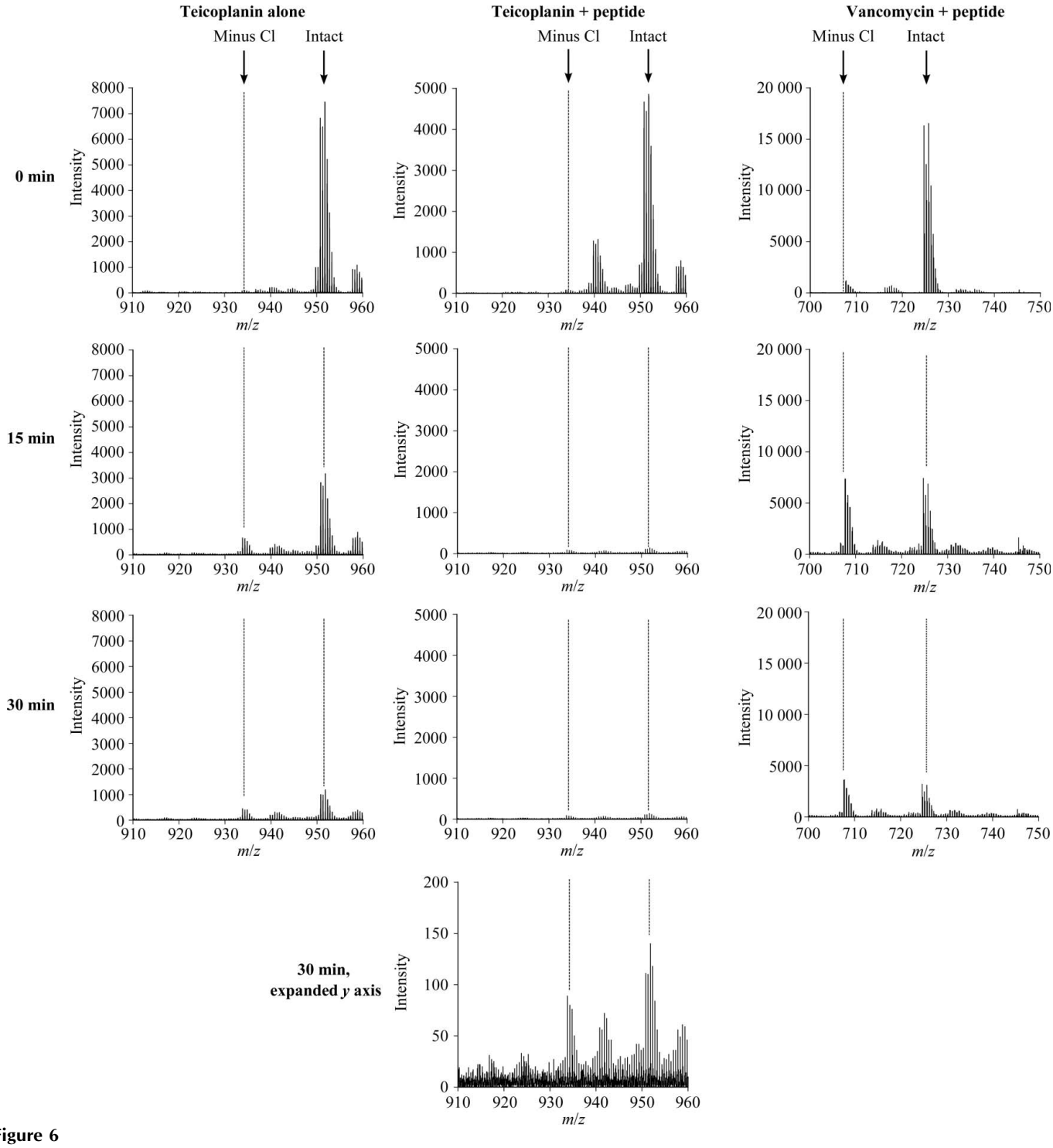

Figure 6
Ligand-induced dechlorination and degradation of teicoplanin in solution. Teicoplanin and vancomycin samples were irradiated for 0, 15 or 30 min and subsequently analyzed by ESI mass spectrometry (NIH/NCRR Mass Spectrometry Resource, Washington University). The samples included teicoplanin alone, teicoplanin with its Ac-Lys-D-Ala-D-Ala ligand and (as a control) vancomycin with the same peptide ligand. For teicoplanin, the portion of the spectrum shown corresponds to the doubly charged $(M + H + Na)^{2+}$ ion, while for vancomycin the spectrum shown corresponds to the doubly charged $(M + 2H)^{2+}$ ion. The positions of the intact and monodechloro ions are indicated (teicoplanin, 1879.66 Da; monodechloro-teicoplanin, 1845.21 Da; vancomycin, 1450.3 Da; monodechloro-vancomycin, 1415.80 Da). At the bottom, the spectrum corresponding to a 30 min exposure of the teicoplanin plus peptide sample is replotted with an expanded scale for the *y* axis to allow the details of the spectrum to be seen.

it is evident that the sugar and fatty-acyl moieties adopt slightly different conformations in the two different environments, which is not surprising given that disorder is frequently associated with such substituents. There is also a small difference in the conformation of the peptide bond for amino acid 3, providing further evidence that this portion of the backbone is inherently flexible.

A surprising finding from this work was the rapid dehalogenation of teicoplanin upon exposure to X-rays. This dehalogenation was observed in two different crystal forms with dissimilar mother liquors and also in a solution with a different composition from either mother liquor. Therefore, the dehalogenation is most likely to be a consequence of an intrinsic hypersensitivity on the part of the molecule and not to any specific solution condition. The residue most affected by dehalogenation is the 3-chlorophenylglycine residue at position 6 of the antibiotic. Many other glycopeptide antibiotics, including vancomycin, balhimycin, avoparcin and dalbavancin, contain an identical residue at this position. Crystal structures have been determined for many of these molecules, but to our knowledge rapid X-ray-induced dehalogenation has only been observed for teicoplanin (this work) and decaplanin (Lehmann *et al.*, 2003).

It is not surprising *per se* that X-ray irradiation can induce dehalogenation. Halogens are expected to be particularly vulnerable to radiation damage owing to their high absorption cross-section; indeed, dehalogenation of brominated nucleotides is commonly encountered in nucleic acid crystallography and is sometimes quite rapid (see, for example, Ravelli *et al.*, 2003; Oliéric *et al.*, 2007; Ennifar *et al.*, 2002). Thus, the X-ray-induced dehalogenation seen with teicoplanin is unusual only because other very similar glycopeptide antibiotics do not share this behavior. The mechanisms underlying site-specific radiation sensitivity are not well understood, but it is believed that the molecular structure of the site plays an important role in determining sensitivity (Holton, 2007). This is consistent with the observation that the chlorine on amino acid 2 is less sensitive to irradiation than its counterpart on amino acid 6: even though they are chemically identical, they exist in different structural environments. It is also consistent with the differential sensitivity observed in the presence *versus* the absence of the ligand, since ligand binding induces structural changes. Interestingly, the Cl atoms on residues 2 and 6 of teicoplanin also show differential sensitivity to reductive dechlorination with $NaBH_4$ and $PdCl_2$ (Malabarba, Spreafico *et al.*, 1989), but in this case the sensitivity is reversed, with the first chlorine removed being that of amino acid 2. Hence, the same structural environment that confers sensitivity to one mechanism of dechlorination appears to offer protection against another. Decaplanin contains only a single chlorine, on residue 2; while appreciable dechlorination was observed for this molecule (Lehmann *et al.*, 2003), the dehalogenation did not approach the essentially complete loss of chlorine that we see at position 6 of teicoplanin, offering additional evidence that Cl atoms attached to amino acid 2 are less vulnerable to radiation damage than their counterparts on amino acid 6.

Because teicoplanin is intrinsically sensitive to X-rays, we would expect any crystal structure including teicoplanin molecules to manifest site-specific dechlorination. However, no mention is made of this in several recent papers describing complexes of teicoplanin with different biosynthetic enzymes (Chan *et al.*, 2011; Liu *et al.*, 2011; Bick *et al.*, 2010). Accordingly, we used the Uppsala Electron-Density Server (Kleywegt *et al.*, 2004) to calculate $2F_o - F_c$ and $F_o - F_c$ maps for PDB entries 2xad, 3mgb and 3mg9. For 2xad there are four copies of the teicoplanin molecule in the asymmetric unit, and for all four copies strong negative $F_o - F_c$ density is seen at the Cl atom of residue 6 but not of residue 2. The $2F_o - F_c$ maps still show some density for the chlorine of residue 6, albeit not as strong as the density for residue 2. Thus, these results are consistent with partial dechlorination at residue 6. Since we do not know the dose associated with this structure determination we cannot directly compare these results with our structures, but they appear to represent a lower level of dechlorination than we observe in our crystal structures. Since no ligand is present in the 2xad structure, this is the result that we would predict based on our solution-irradiation experiments, which showed reduced radiation sensitivity for ligand-free samples relative to antibiotic ligand complexes. In both the 3mg9 and 3mgb cases there are two copies of the teicoplanin molecule in the asymmetric unit. In both structures at least one of the two molecules in the asymmetric unit shows signs suggesting radiation damage (either very high atomic displacement parameters or zero occupancies). In both structures the damage does not appear to be equal for both molecules in the asymmetric unit. Importantly, the 3mg9 and 3mgb structures differ from the structure reported in this paper and from 2xad in that 3mg9 and 3mgb contain the aglycon form of teicoplanin, that is, antibiotic lacking all sugar and acyl substituents; it is certainly possible that the carbohydrate and lipid groups of the antibiotic play important roles in controlling site-specific radiation sensitivity.

Given that our teicoplanin structures represent non-native dechlorinated forms of the molecule, it is important to ask whether these structures accurately reflect the structure of the native fully chlorinated antibiotic. Two arguments suggest that this structure is indeed relevant. Firstly, while the Cl atoms are known to contribute to ligand binding, they are not absolutely required. The affinity of the fully dechlorinated form of teicoplanin for its ligand is reduced approximately 15-fold (Malabarba, Trani *et al.*, 1989). No binding data are available for the form of the antibiotic lacking the chlorine at amino acid 6; however, presumably it binds ligand at least as well, or better, than the di-dechloro form and thus retains its function. Secondly, we can examine the structures of related molecules that have not undergone dechlorination. Of all glycopeptide antibiotics of known structure, dalbavancin is most similar to teicoplanin. Superposition of teicoplanin and dalbavancin shows that the two molecules are very similar in structure, even around the site of dechlorination (Fig. 3), indicating that dechlorination has probably not significantly altered the structure of teicoplanin.

In conclusion, we have used a carrier-protein strategy to determine the first crystal structure of teicoplanin bound to its antimicrobial target. This work has revealed a previously unremarked flexibility of the backbone of the antibiotic and has provided new insights into how glycopeptides bind their targets that may prove useful for the design of improved antibacterials.

We gratefully acknowledge the Cold Spring Harbor course 'X-ray Methods in Structural Biology'. This research was supported by grant R01GM079508 (NIH/NIGMS). Diffraction data were collected on beamline NE-CAT 24-IDE of the Advanced Photon Source at Argonne National Laboratory and beamlines X6A and X25 of the National Synchrotron Light Source. Financial support for the NSLS beamlines comes principally from the Offices of Biological and Environmental Research and of Basic Energy Sciences of the US Department of Energy and from the National Institute of General Medical Sciences of the National Institutes of Health.

References

Adams, P. D. *et al.* (2010). *Acta Cryst.* D**66**, 213–221.
Arriaga, P., Laynez, J., Menendez, M., Cañada, J. & Garcia-Blanco, F. (1990). *Biochem. J.* **265**, 69–77.
Arthur, M., Molinas, C., Bugg, T. D., Wright, G. D., Walsh, C. T. & Courvalin, P. (1992). *Antimicrob. Agents Chemother.* **36**, 867–869.
Barna, J. C. & Williams, D. H. (1984). *Annu. Rev. Microbiol.* **38**, 339–357.
Beauregard, D. A., Williams, D. H., Gwynn, M. N. & Knowles, D. J. (1995). *Antimicrob. Agents Chemother.* **39**, 781–785.
Bick, M. J., Banik, J. J., Darst, S. A. & Brady, S. F. (2010). *Biochemistry*, **49**, 4159–4168.
Borghi, A., Coronelli, C., Faniuolo, L., Allievi, G., Pallanza, R. & Gallo, G. G. (1984). *J. Antibiot.* **37**, 615–620.
Bravman, T., Bronner, V., Lavie, K., Notcovich, A., Papalia, G. A. & Myszka, D. G. (2006). *Anal. Biochem.* **358**, 281–288.
Bugg, T. D., Wright, G. D., Dutka-Malen, S., Arthur, M., Courvalin, P. & Walsh, C. T. (1991). *Biochemistry*, **30**, 10408–10415.
Center, R. J., Kobe, B., Wilson, K. A., Teh, T., Howlett, G. J., Kemp, B. E. & Poumbourios, P. (1998). *Protein Sci.* **7**, 1612–1619.
Chan, H.-C., Huang, Y.-T., Lyu, S.-Y., Huang, C.-J., Li, Y.-S., Liu, Y.-C., Chou, C.-C., Tsai, M.-D. & Li, T.-L. (2011). *Mol. Biosyst.* **7**, 1224–1231.
Chen, V. B., Arendall, W. B., Headd, J. J., Keedy, D. A., Immormino, R. M., Kapral, G. J., Murray, L. W., Richardson, J. S. & Richardson, D. C. (2010). *Acta Cryst.* D**66**, 12–21.
Colombo, L., Malabarba, A. & Stogniew, M. (2009). US Patent Application 20090305953.
Cooper, M. E., Williams, D. H. & Cho, Y. R. (1997). *Chem. Commun.*, pp. 1625–1626.
Corti, A., Soffientini, A. & Cassani, G. (1985). *J. Appl. Biochem.* **7**, 133–137.
DeLano, W. L. (2002). *PyMOL*. http://www.pymol.org.
Derewenda, Z. S. (2010). *Acta Cryst.* D**66**, 604–615.
Duan, X. & Quiocho, F. A. (2002). *Biochemistry*, **41**, 706–712.
Dutka-Malen, S., Leclercq, R., Coutant, V., Duval, J. & Courvalin, P. (1990). *Antimicrob. Agents Chemother.* **34**, 1875–1879.
Economou, N. J., Nahoum, V., Weeks, S. D., Grasty, K. C., Zentner, I. J., Townsend, T. M., Bhuiya, M. W., Cocklin, S. & Loll, P. J. (2012). *J. Am. Chem. Soc.* **134**, 4637–4645.
Emsley, P., Lohkamp, B., Scott, W. G. & Cowtan, K. (2010). *Acta Cryst.* D**66**, 486–501.
Engh, R. A. & Huber, R. (1991). *Acta Cryst.* A**47**, 392–400.
Ennifar, E., Carpentier, P., Ferrer, J.-L., Walter, P. & Dumas, P. (2002). *Acta Cryst.* D**58**, 1262–1268.
Evans, T. C. Jr, Benner, J. & Xu, M.-Q. (1998). *Protein Sci.* **7**, 2256–2264.
Handwerger, S., Pucci, M. J., Volk, K. J., Liu, J. & Lee, M. S. (1992). *J. Bacteriol.* **174**, 5982–5984.
Heald, S. L., Mueller, L. & Jeffs, P. W. (1987). *J. Magn. Reson.* **72**, 120–138.
Holton, J. M. (2007). *J. Synchrotron Rad.* **14**, 51–72.
Kabsch, W. (2010). *Acta Cryst.* D**66**, 125–132.
Kahne, D., Leimkuhler, C., Lu, W. & Walsh, C. (2005). *Chem. Rev.* **105**, 425–448.
Kalman, J. R. & Williams, D. H. (1980). *J. Am. Chem. Soc.* **102**, 906–912.
Kleywegt, G. J., Harris, M. R., Zou, J., Taylor, T. C., Wählby, A. & Jones, T. A. (2004). *Acta Cryst.* D**60**, 2240–2249.
Kleywegt, G. J. & Jones, T. A. (1998). *Acta Cryst.* D**54**, 1119–1131.
Kobe, B., Center, R. J., Kemp, B. E. & Poumbourios, P. (1999). *Proc. Natl Acad. Sci. USA*, **96**, 4319–4324.
Koide, S. (2009). *Curr. Opin. Struct. Biol.* **19**, 449–457.
Lehmann, C., Debreczeni, J., Bunkóczi, G., Dauter, M., Dauter, Z., Vértesy, L. & Sheldrick, G. (2003). *Helv. Chim. Acta*, **86**, 1478–1487.
Liu, Y.-C., Li, Y.-S., Lyu, S.-Y., Hsu, L.-J., Chen, Y.-H., Huang, Y.-T., Chan, H.-C., Huang, C.-J., Chen, G.-H., Chou, C.-C., Tsai, M.-D. & Li, T.-L. (2011). *Nature Chem. Biol.* **7**, 304–309.
Loll, P. J. & Axelsen, P. H. (2000). *Annu. Rev. Biophys. Biomol. Struct.* **29**, 265–289.
Loll, P. J., Bevivino, A. E., Korty, B. D. & Axelsen, P. H. (1997). *J. Am. Chem. Soc.* **119**, 1516–1522.
Malabarba, A. & Goldstein, B. P. (2005). *J. Antimicrob. Chemother.* **55**, ii15–ii20.
Malabarba, A., Nicas, T. & Ciabatti, R. (1997). *Eur. J. Med. Chem.* **32**, 459–478.
Malabarba, A., Nicas, T. I. & Thompson, R. C. (1997). *Med. Res. Rev.* **17**, 69–137.
Malabarba, A., Spreafico, F., Ferrari, P., Kettenring, J., Strazzolini, P., Tarzia, G., Pallanza, R., Berti, M. & Cavalleri, B. (1989). *J. Antibiot.* **42**, 1684–1697.
Malabarba, A., Trani, A., Tarzia, G., Ferrari, P., Pallanza, R. & Berti, M. (1989). *J. Med. Chem.* **32**, 783–788.
Moon, A. F., Mueller, G. A., Zhong, X. & Pedersen, L. C. (2010). *Protein Sci.* **19**, 901–913.
Morris, R. J. & Bricogne, G. (2003). *Acta Cryst.* D**59**, 615–617.
Muir, T. W. (2003). *Annu. Rev. Biochem.* **72**, 249–289.
Nahoum, V., Spector, S. & Loll, P. J. (2009). *Acta Cryst.* D**65**, 832–838.
Nieto, M. & Perkins, H. R. (1971*a*). *Biochem. J.* **123**, 789–803.
Nieto, M. & Perkins, H. R. (1971*b*). *Biochem. J.* **124**, 845–852.
Novotna, G., Hill, C., Vincent, K., Liu, C. & Hong, H.-J. (2012). *Antimicrob. Agents Chemother.* **56**, 1784–1796.
Oliéric, V., Ennifar, E., Meents, A., Fleurant, M., Besnard, C., Pattison, P., Schiltz, M., Schulze-Briese, C. & Dumas, P. (2007). *Acta Cryst.* D**63**, 759–768.
Owen, R. L., Holton, J. M., Schulze-Briese, C. & Garman, E. F. (2009). *J. Synchrotron Rad.* **16**, 143–151.
Paithankar, K. S., Owen, R. L. & Garman, E. F. (2009). *J. Synchrotron Rad.* **16**, 152–162.
Parenti, F. (1986). *J. Hosp. Infect.* **7**, *Suppl. A*, 79–83.
Perkins, H. R. (1969). *Biochem. J.* **111**, 195–205.
Popieniek, P. H. & Pratt, R. F. (1991). *J. Am. Chem. Soc.* **113**, 2264–2270.
Ravelli, R. B. G., Leiros, H.-K. S., Pan, B., Caffrey, M. & McSweeney, S. (2003). *Structure*, **11**, 217–224.
Schäfer, M., Schneider, T. R. & Sheldrick, G. M. (1996). *Structure*, **4**, 1509–1515.
Schüttelkopf, A. W. & van Aalten, D. M. F. (2004). *Acta Cryst.* D**60**, 1355–1363.

Scrimin, P., Tecilla, P., Tonellato, U., Verzini, M., Andreini, B. P., Coutant, J. E. & Zerilli, L. F. (1996). *J. Org. Chem.* **61**, 6268–6272.
Sheldrick, G. M. (1990). *Acta Cryst.* A**46**, 467–473.
Sheldrick, G. M., Paulus, E., Vértesy, L. & Hahn, F. (1995). *Acta Cryst.* B**51**, 89–98.
Usón, I. & Sheldrick, G. M. (1999). *Curr. Opin. Struct. Biol.* **9**, 643–648.
Vagin, A. & Teplyakov, A. (2010). *Acta Cryst.* D**66**, 22–25.
Verbist, L., Tjandramaga, B., Hendrickx, B., Van Hecken, A., Van Melle, P., Verbesselt, R., Verhaegen, J. & De Schepper, P. J. (1984). *Antimicrob. Agents Chemother.* **26**, 881–886.
Vijay-Kumar, S., Bugg, C. E. & Cook, W. J. (1987). *J. Mol. Biol.* **194**, 531–544.
Walsh, C. (2003). *Antibiotics: Actions, Origins, Resistance.* Washington: ASM Press.
Waltho, J. P. & Williams, D. H. (1989). *J. Am. Chem. Soc.* **111**, 2475–2480.
Westwell, M. S., Bardsley, B., Dancer, R. J., Try, A. C. & Williams, D. H. (1996). *Chem. Commun.*, pp. 589–590.
Westwell, M. S., Gerhard, U. & Williams, D. H. (1995). *J. Antibiot.* **48**, 1292–1298.